GROUND-BASED LASER SCANNERS: OPERATION, SYSTEMS AND APPLICATIONS

D.D. Lichti, S.J. Gordon and M.P. Stewart
Department of Spatial Sciences, Curtin University of Technology, Perth, Australia

Ground-based laser scanning is a new technology available to photogrammetrists, geodesists and surveyors for rapid and extremely dense spatial data capture. This paper describes some of the fundamentals of scanner operation, followed by a review of the salient properties of five commercially available scanner systems. Scanner geometry, observables and associated co-ordinate transformations are then detailed. Several case studies selected from research conducted at Curtin University are described to complete the paper.

Le balayage laser au sol est une nouvelle technologie disponible pour les photogrammètres, les géodésiens et les arpenteurs pour la saisie rapide de données spatiales extrêmement denses. Cet article décrit certains éléments fondamentaux du balayage et donne un aperçu des principales propriétés de cinq systèmes de balayage disponibles sur le marché. La géométrie des balayeurs, les observations et les transformations des coordonnées associées sont ensuite précisées. Plusieurs études de cas sélectionnées de la recherche entreprise à l'Université Curtin sont décrites pour compléter l'article.

Introduction

Ground-based laser scanning is an emerging technology offering great potential for rapid collection of dense, three-dimensional (3D) spatial datasets of entire surfaces. Traditional methods of spatial data capture, which include surveying and photogrammetric techniques, suffer from several shortcomings. While very accurate, they offer only limited data coverage at a few discrete points on a measurement surface. As these methods are somewhat labour intensive, data acquisition is time consuming and, therefore, costly.

On the other hand, a laser scanner can provide very dense 3D co-ordinate measurements. The fine angular sampling interval, which ranges from a few microradians to a few milliradians, allows capture of several millions of points over an entire surface. For example, a 5 μrad angular interval at a range of 50 m equates to a 0.25 mm sample interval, or 16 million point measurements/m^2. For a 5 mrad angular interval, the sample interval is 0.25 m and point density is 16 measurements/m^2. Data collection rates can exceed several thousand points per second, which allows entire surfaces or structures to be measured in a matter of minutes. At the time of writing (May 2001), the drawback to this new technology is the high cost of the hardware.

Applications of ground-based laser scanning are only limited by one's imagination. Initial projects conducted by the authors include deformation monitoring of a large structure (a rock fill dam), structural assessment of an ageing timber bridge, subsidence monitoring of a building and measurement of a granite quarry. The advantages of laser scanning for these projects are the non-contact measurement, rapid acquisition rate and dense data coverage.

Other potential applications that can benefit from the dense spatial data coverage include as-built surveys of industrial process plants that consist of many pipes, machines and structural members. Laser scanners can also provide the high spatial resolution required for architectural restoration of intricately detailed building facades. Another potential application is automobile accident scene recording, which requires rapid 3D mapping of a crash site so that normal traffic flow can resume with minimal delay. Within the mining industry exist numerous possibilities, from stope stability monitoring to stockpile measurement to open pit site rehabilitation.

This paper reviews the current status of ground-based laser scanning technology. Basic scanner operation is first discussed. Five commercially available scanners are then described in terms of their properties relevant to photogrammetrists and surveyors, including resolution, accuracy, maximum range and operational characteristics. This is followed by discussion of scanner geometry, observables, and transformations required to georeference point clouds. Finally, a summary is given of ground-based laser scanning projects conducted at Curtin University.

Laser Scanner Operation

All ground-based laser scanners reviewed in this article measure range by the pulse method. Other methods not reviewed here include continuous-wave ranging [*Wehr and Lohr* 1999] and triangulation [*Beraldin et al.* 2000]. To measure by the pulse method, the scanner emits a brief pulse of laser light, which, after reflection by the object being measured, is sensed by a photodetector. The range, ρ, is derived from the two-way flight time of the pulse, Δt, via

$$\rho = \frac{1}{2} c\Delta t \qquad (1)$$

where c is the velocity of light. Three-dimensional measurement is facilitated by two rotational degrees of freedom. Rotating mirrors and/or servomechanisms deflect the laser pulse in equal intervals of arc in both horizontal and vertical planes. Figure 1 illustrates the concept of laser scanner measurement.

Pulsed laser scanners are reflectorless systems, meaning a corner cube prism or other reflector is unnecessary for range measurement. The energy of the reflected pulse depends on both physical and geometric factors. Physical factors include the reflecting material's electric permittivity, magnetic permeability and conductivity [*Fowles* 1975; *Jelalian* 1992], all of which are wavelength dependent. These parameters determine how much of the pulse's energy is absorbed by the reflecting surface. Geometric factors include the angle of incidence and surface roughness, which determine how the incident radiation is scattered.

Time of flight is derived once the return pulse amplitude crosses an internally defined threshold. Considering for the moment measurement of smooth surfaces at normal incidence, and neglecting atmospheric effects, return pulse amplitude is a function of the material properties, which differ from surface to surface. A pulse with reduced amplitude crosses the detection threshold slightly later than the full amplitude pulse [*Baltsavias* 1999]. This time delay, δt, gives rise to a range delay, δr, as per Equation 1, i.e.

$$\delta\rho = \frac{1}{2} c\delta t \qquad (2)$$

Quantification of this effect for different reflecting materials is the subject of continuing research at Curtin University.

In addition to range and angular measurements, most systems also offer a quantised measure of return signal amplitude, often loosely termed intensity. Intensity can give insight into the material properties of the reflecting surface. Unfortunately, the physical significance of this attribute, i.e. whether it indicates return pulse amplitude or energy, is often not explicitly stated by the scanner manufacturers.

The beam diameter or footprint size is a function of the laser wavelength, range and beam waist diameter. After emission, the beam diameter actually decreases to a minimum called the beam waist. Beyond the beam waist, the beam diverges according to [*Weichel* 1990]

$$w(z) = w_0\sqrt{1 + \left(\frac{\lambda z}{\pi w_0^2}\right)^2} \qquad (3)$$

where

$w(z)$	is the beam radius at range z;
z	is the range from the beam waist;
w_0	is the beam waist radius; and
λ	is the central laser wavelength.

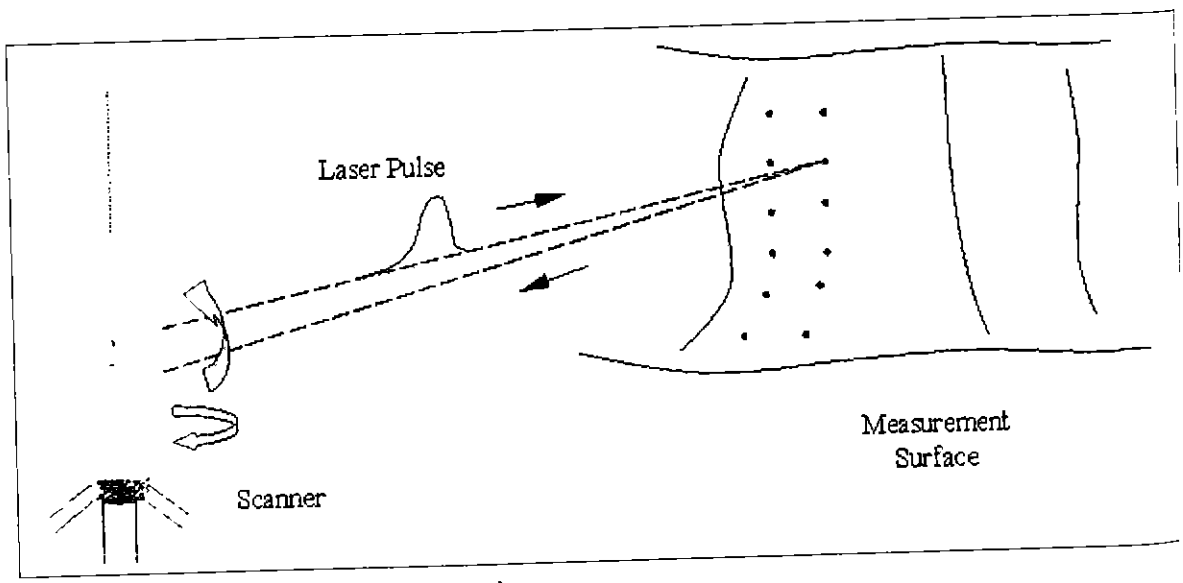

Figure 1: Ground-based laser scanner operation.

For large ranges, divergence is approximately linear and is specified by an angular quantity, γ, in mrad. Analysis of Equation 3 indicates that beam divergence is greater for a beam with a small waist, the diameter of which is controlled by the scanner optics. Additionally, beam diameter is smaller for shorter wavelengths and, thus, the spatial resolution of the scanner is higher.

The irradiance (power per unit area) distribution within the footprint is not uniform, but is Gaussian. Several definitions for beam diameter exist, such as half-beam power diameter, $1/e^2$ irradiance level diameter, and full-power ($1/e^8$) beam diameter, for which the fraction of the encircled beam power is 50%, 86% and 99.97% of the total power, respectively [*Marshall* 1985]. The most common is the $1/e^2$ beam diameter definition [*Matthews and Garcia* 1995]. Figure 2, which illustrates beam waist and divergence, also schematically shows the Gaussian shape of the beam irradiance distribution for the cross-section AA'.

Laser scanners are fundamentally different from surveying instruments in that they are not pointable measuring devices. With a total station, for example, range measurement to a point is performed unambiguously by placing the telescope crosshairs on the centre of a target. This is not the case with a laser scanner, which measures range in uniform increments of arc. Although not a problem for surface measurements, it poses a challenge for benchmark testing in which targeted control points are used. Instead of a single measurement, a highly reflective target—the preferred target for such testing—returns a cluster of responses that must be reduced to a position estimate for the centre. Preliminary research has identified this as a possible systematic error source in benchmark testing [*Lichti et al.* 2000].

Scanner Systems

Several ground-based laser-scanning systems are currently available. These vary in construction, operation, maximum range, accuracy, resolution and central laser wavelength. Systems also vary in size, with new generations of the hardware becoming progressively more compact. Most allow interactive selection of the scan area through digital imagery captured with an on-board video camera. Some systems have levelling, forced centring and scanner orientation establishment capabilities. In spite of the differences, all the systems discussed are based upon the same measurement principles outlined in the previous section. All systems are driven by proprietary software. A summary of some of the properties of four scanner systems is provided in Table 1.

The I-SiTE 3D Laser Imaging system from Australia uses the RIEGL scanner (described below) and offers range measurements of up to 350 m provided surface reflectance is greater than 50% [*I-SiTE* 2001]. The Class 1 laser operates in the near infrared (NIR) portion of the spectrum with a central wavelength of 900 nm. Scanning can be performed through a horizontal range of 340° and a vertical range of ± 40°. The instrument can be levelled and force-centred. Both accuracy and resolution are quoted at ± 25 mm, although since spatial resolution is range dependent, this figure is possibly intended to represent accuracy. Range measurement up to 700 m is also possible, but with a lower accuracy of ± 50 mm. At the time of writing, no information was posted on the I-SiTE Web site concerning angular resolution. However, three resolutions were available when the authors hired the instrument in late 1999: fine, medium and coarse. The angular resolution of the fine mode was approximately 2 mrad. Other parameters of interest are the 6 kHz data acquisition rate and 3 mrad beam divergence.

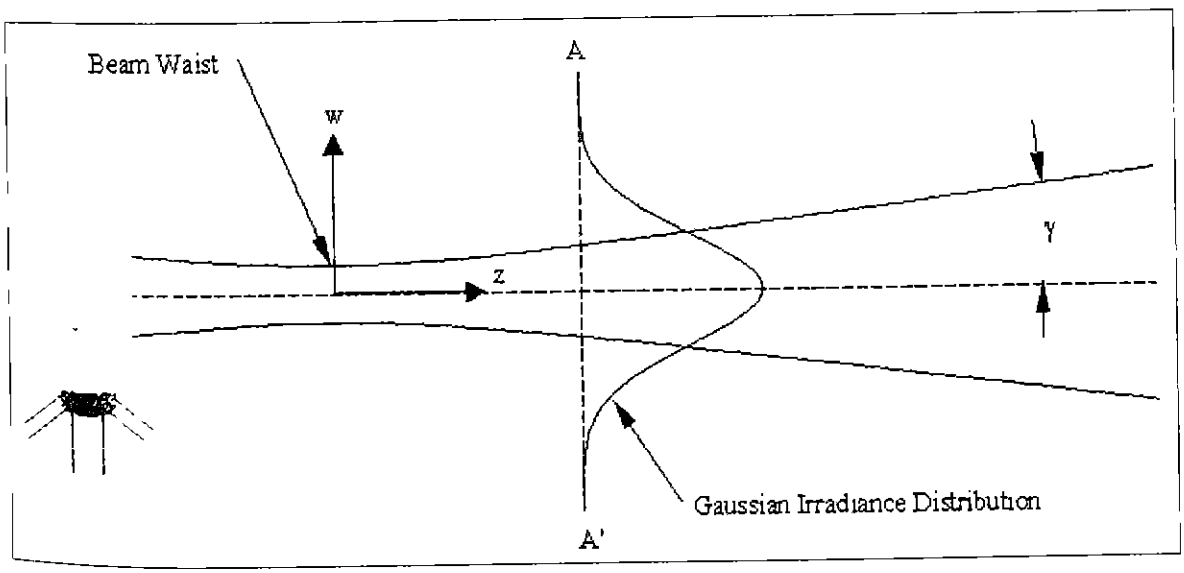

Figure 2: Beam waist, divergence and irradiance distribution.

Table 1: Summary of some Laser Scanner System Characteristics.

	RIEGL LMS-Z210 and I-SiTE	Cyrax 2500	Callidus	Optech ILRIS-3D
Accuracy	Maximum range dependent: ± 25 mm up to 350 m ± 50 mm up to 700 m	± 6 mm	± 5 mm	±10 mm
Maximum Range	350 m or 700 m	100 m	32 m, 80 m or 100 m	800 m
Scan Rate	6 kHz	1 kHz	2.7 kHz	2 kHz
Angular Resolution	Fine, medium or coarse Fine: ≈ 2 mrad	Variable: To 0.25 mm at 50 m	Variable: 0.0625° to 1°	Variable: < 20 mm at 100 m
Field of View	H: 340° V: 80	H: 40° V: 40°	H: 360° V: 150°	H: 40° V: 40°
Laser	Class 1 NIR	Class 2 Green	Class 1 NIR	Class 1 NIR
Beam Divergence or Spot Size	3 mrad	< 6 mm at 50 m	0.25°	20 mm at 100 m
Scanner Orientation	Tribrach with level bubbles and optical plummet; optical scope	3D Resection	Mount on top for prism or GPS antenna; inclination sensors; electronic magnetic compass	3D Resection

The LMS-Z210 3D Imaging Sensor from the Austrian firm RIEGL is the instrument at the core of the I-SiTE system. The RIEGL Web site provides more comprehensive technical specifications for resolution and accuracy [*RIEGL* 2001]. Interestingly, RIEGL provides a description of a series of environmental tests performed on the LMS-Z210, including operation at various temperatures and under different dynamic loading conditions (e.g. shock and vibration). This information would be of interest for applications in hazardous environments such as industrial plants where high temperatures and excessive vibration could affect instrument operation.

The Cyrax 2500 from Cyra Technologies of the U.S. offers range measurements of up to 100 m with a Class 2 green laser (the central wavelength is 532 nm). The Cyrax's scanning resolution is relatively high, with a maximum of 0.25 mm at a range of 50 m, which equates to a 5 µrad angular resolution. Data acquisition rates vary with the programmable sampling rate. Single-point accuracy is quoted at $\sigma = \pm 6$ mm for ranges between 1.5 m and 50 m, while for a subsequently modelled surface, $\sigma =$ ± 2 mm is stated. Both the horizontal and vertical fields of view are 40°. Although beam divergence is not directly given at the Cyra Web site, the laser spot size is quoted as less than 6 mm over the range of 0 to 50 m. The surveying industry's interest in laser scanning is perhaps best indicated by Leica Geosystems' acquisition of Cyra [*Cyra* 2001].

The Callidus 3D Laser System is a German instrument offering variable maximum range and resolution. Three different operation modes are available for different applications: maximum range up to 8 m, 32 m, and 80 m [*Callidus* 2001]. Several angular resolutions are available, ranging from 0.0625° (≈1.1 mrad) to 1° (≈17 mrad). This system features a full 360° horizontal field of view. Surface accuracy rather than single-point accuracy is emphasized, and is quoted at ± 5 mm. The Callidus uses a Class 1 NIR ($\lambda = 906$ nm) laser for range measurement. The instrument is fitted with inclination sensors, electronic compass and prism mount atop the scanner for georeferencing.

The Optech ILRIS-3D Lidar Imaging System from Canada can measure ranges up to 800 m at 20% reflectance or 350 m with 4% reflectance [*Optech*

2001]. Range resolution is quoted as ± 10 mm. The ILRIS-3D point sampling rate is 2 kHz and both the horizontal and vertical fields of view are 40°. The sample spacing (e.g. angular resolution) is variable. The laser is quoted as being eye safe under all operating conditions. ILRIS-3D features first and last pulse measurement modes that permit omission of unwanted laser returns in the background or foreground, respectively.

Observables and Transformations

The geometry of terrestrial laser scanning is depicted in Figure 3. The scanner observables are range, ρ, elevation angle, α, (or, equivalently, zenith angle) and horizontal direction, θ, which are made relative to the scanner's internally defined co-ordinate system (scanner space). Cartesian co-ordinates, (x, y, z), are the quantities provided as output from most scanner software packages and are usually treated as observables. This parameterization also simplifies the transformation equations required for georeferencing scanner point clouds.

The georeferencing problem in the laser-scanning context involves transforming the observables from scanner space to object space. Object space may be a local or a global co-ordinate system realized by a set of 3D control points. The rigid-body transformation of an observed vector from scanner space to object space is given by

$$\vec{R}_p = M\vec{r}_p + \vec{R}_s \tag{4}$$

where

$\vec{r}_p = [x_p\ y_p\ z_p]^T$ is the observed position vector of point p in scanner space;

$\vec{R}_p = [X_p\ Y_p\ Z_p]^T$ is the position vector of point p in object space;

$\vec{R}_s = [X_s\ Y_s\ Z_s]^T$ is the position vector of the scanner space origin in object space;

and

M is the rotation matrix of three sequential angles (ω, ϕ, κ) about the X-, Y- and Z-axes, respectively, and is given by

$$M = \begin{bmatrix} \cos\phi\cos\kappa & \cos\omega\sin\kappa+\sin\omega\sin\phi\cos\kappa & \sin\omega\sin\kappa-\cos\omega\sin\phi\cos\kappa \\ -\cos\phi\sin\kappa & \cos\omega\cos\kappa-\sin\omega\sin\phi\sin\kappa & \sin\omega\cos\kappa+\cos\omega\sin\phi\sin\kappa \\ \sin\phi & -\sin\omega\cos\phi & \cos\omega\cos\phi \end{bmatrix} \tag{5}$$

Unique solution of the translation parameters (X_S, Y_S, Z_S) and rotation angles (ω, ϕ, κ) requires a

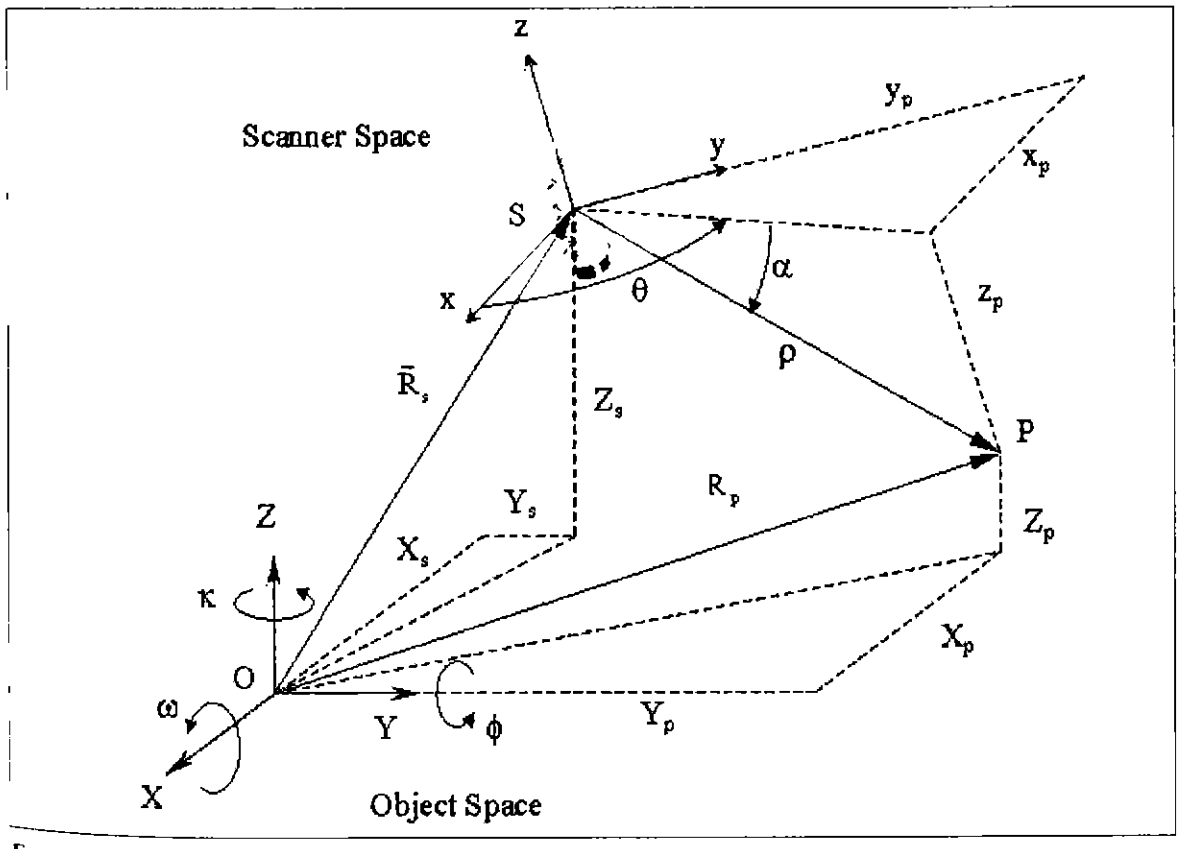

Figure 3: Laser scanning geometry.

combination of six co-ordinate observations from three non-collinear object space points. Usually, three or more full control points are available and least-squares estimation used to determine a unique set of parameter estimates. For parametric model implementation, Equation 4 can be rearranged in terms of the observables as

$$\vec{r}_p = M^T \left(\vec{R}_p - \vec{R}_s \right) \tag{6}$$

Strictly speaking, the covariance matrix of the derived observables, (x_p, y_p, z_p), should be determined from that of $(\rho_p, \alpha_p, \theta_p)$ through variance propagation. This matrix is block diagonal comprising full 3x3 matrices. However, a diagonal structure is often assumed to simplify formation of the normal equations and post-adjustment reliability analysis.

The ability to level, force centre and orient a scanner reduces the complexity of georeferencing. With reference to Figure 3, levelling the scanner sets both the tilt angles, ω and ϕ, to zero. Forced-centring over a known point or direct position measurement via total station or GPS provides the three translation parameters. The κ rotation angle can be set by orientation measurement with an external sensor, such as a theodolite or total station integrated with the scanning system.

Case Studies at Curtin University

The Department of Spatial Sciences at Curtin University of Technology has been conducting ground-based laser scanning research since 1999. The main focus of this work has been structural monitoring in a variety of environments. A synopsis of projects is provided below.

North Dandalup Dam

The North Dandalup dam complex, located about 70 km south of Perth, Western Australia, is monitored for the West Australian Water Corporation at three-month intervals using a combination of GPS and precise levelling methods. The monitoring criteria are very stringent, with an absolute accuracy of ± 5 mm and ± 2 mm required in planimetry and height, respectively. The main dam, illustrated in Figure 4, is of earth-fill construction and is some 60 m high and 500 m long. Laser scanning of the structure with the I-SITE system commenced in September 1999 to assess the feasibility of this technology for structural monitoring. A plan view of one of the scan clouds is shown in Figure 5.

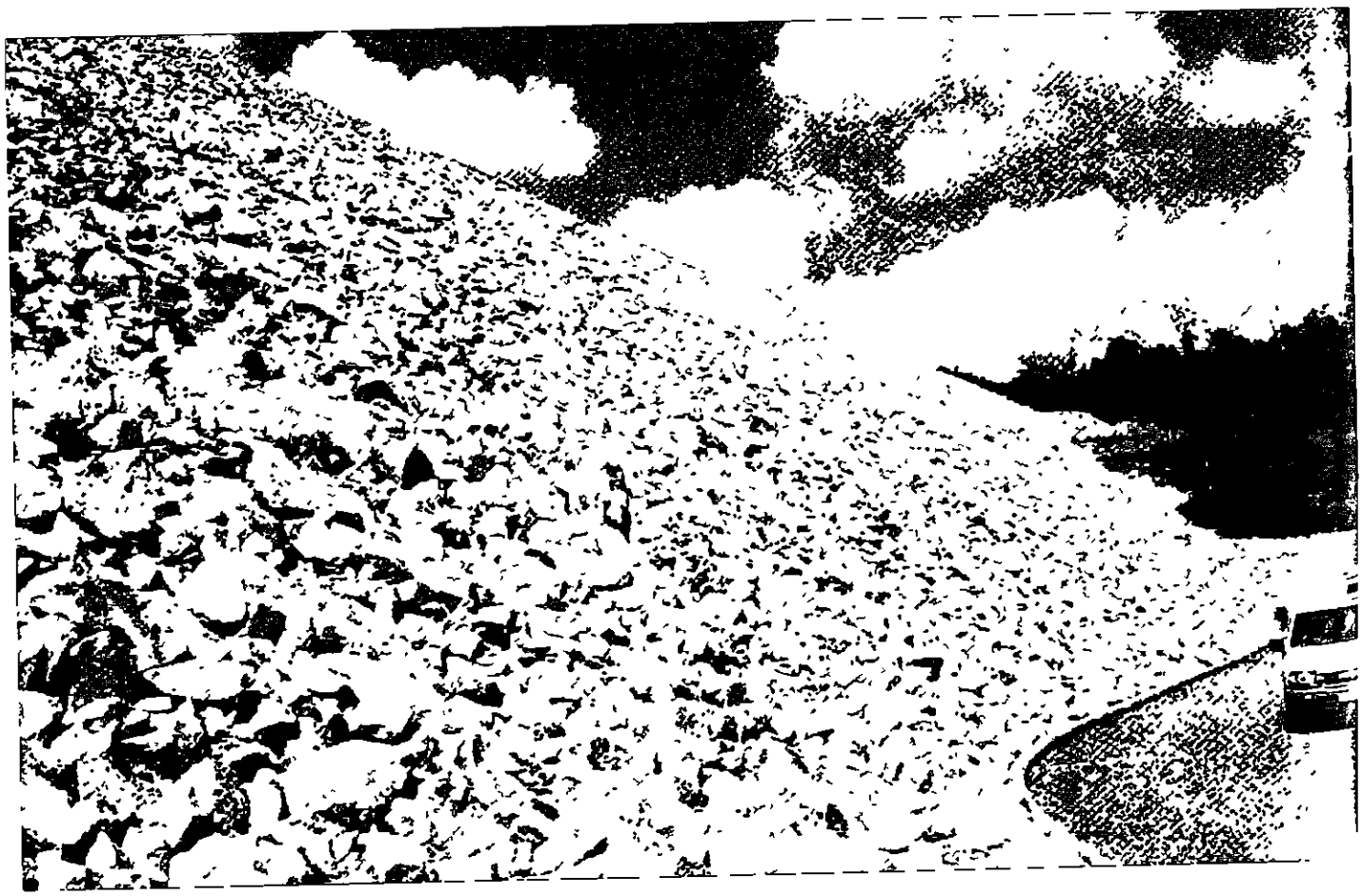

Figure 4 North Dandalup Dam.

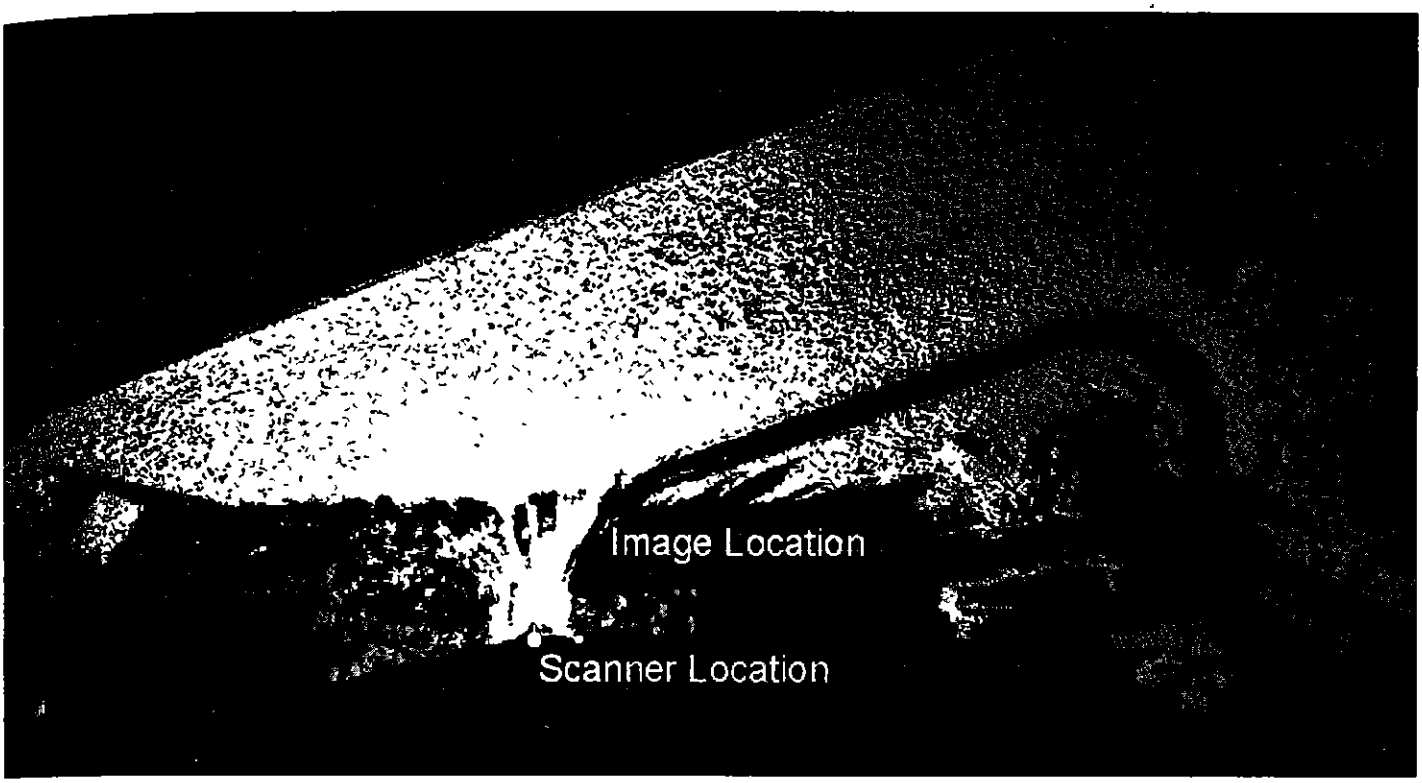

Figure 5: Plan view of a North Dandalup Dam scan cloud.

which indicates both the scanner location and position from which the image in Figure 4 was captured. The access road running across the face of the dam is clearly visible, as is the top of the dam. Notice that the sample density decreases with distance from the scanner location due to the equal angle interval sampling. The grey value of each sample represents the quantised return signal strength.

The testing involved scanning the dam from three different locations below the structure. Two scans were acquired at each location, making a total of six. Data capture over the dam surface was quick, as each scan took only a matter of minutes. The scanned field of view was approximately 150° with a sample interval of 2 mrad. A set of pre-surveyed monitoring points on the dam was targeted with low-cost reflectors. The co-ordinates of these targets, determined by GPS and levelling to $\sigma \leq \pm 5$ mm in each dimension, served as an independent dataset against which scanner performance could be gauged.

After reduction of the cluster of returns from each target to a centroid estimate, each scanner dataset was georeferenced via rigid-body transformation (Equation 4). Both repeatability and accuracy were assessed. Scanner co-ordinate repeatability was up to ± 6.6 cm (1 σ), with mean values up to 2.1 cm. Co-ordinate accuracy, assessed by comparing transformed and "known" co-ordinates, was found to be up to ± 4.3 cm (1 σ). While these figures appear to be more pessimistic than those claimed by the scanner manufacturer, the authors acknowledge that they are contaminated with systematic errors due to centroid reduction and errors in the "known" co-ordinates. Further details on the results of this experiment are found in *Lichti et al.* [2000].

Toodyay Bridge 631

Toodyay bridge 631 spans the Avon river on the outskirts of Toodyay, Western Australia, approximately 90 km northeast of Perth. Shown in Figure 6, the single-lane bridge is approximately 190 m long and is of timber construction with a concrete deck. The ageing structure has been fortified in several places with additional timber members and steel I-beams. At the time of writing (May 2001), construction of a replacement bridge was well underway. Upon completion of the replacement, the existing bridge is to be destructively tested and dismantled. This testing will provide validation of structural models for the bridge constructed on the basis of field measurements.

The finite element structural model of the bridge requires knowledge of both its physical and its geometric properties. The physical characteristics are the material properties (e.g. Young's modulus of elasticity, Poisson's ratio, etc.) of the individual members and bridge deck. Geometric properties include the position and dimensions (e.g. length, cross-sectional area, etc.) of the members.

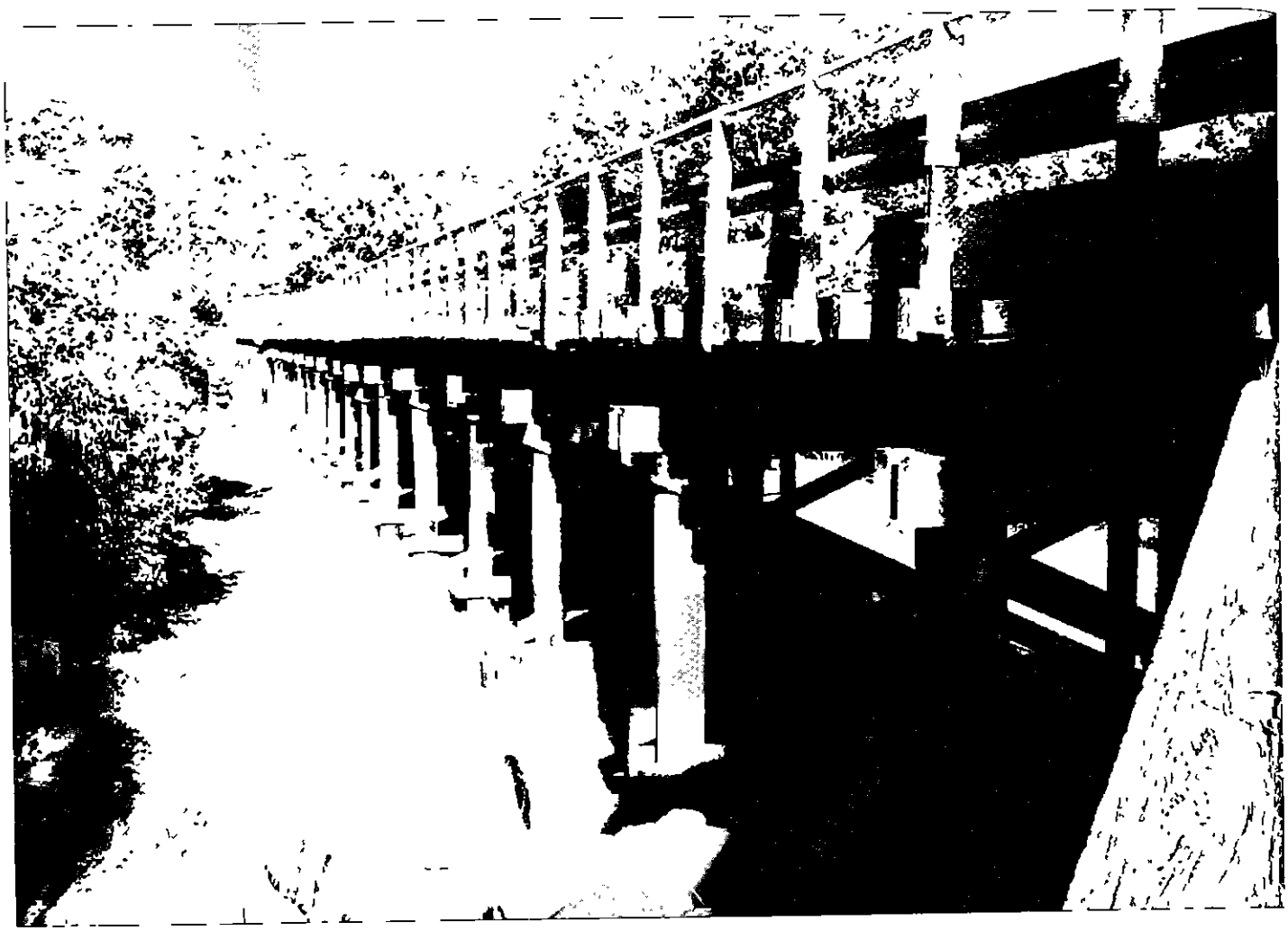

Figure 6. Toodyay bridge 631

The Cyrax 2400 (predecessor to the 2500) was used to obtain the geometric properties of the bridge in May 2000. Scanning was performed from five locations on one side of the bridge with a spatial resolution of 15 mm at 15 m (1 mrad). Each cloud was transformed to a local co-ordinate system defined by pre-surveyed, proprietary Cyra targets and filtered to remove unwanted returns from surrounding vegetation and the ground. The resulting scan cloud mosaic, shown in Figure 7, effectively captures the intricate details of the bridge.

Due to the long scan time demanded by the high spatial resolution required for the job, only about 25% of the bridge was imaged. Data coverage was also an issue, as some members occluded others. Figure 8, which is a portion of an extracted I-beam, exemplifies the shadowing effect. Several gaps exist in the point cloud of the beam due to occlusion by wooden cross-braces. Shadow effects are also visible in the entire mosaic (see Figure 7). The three section views in Figure 8 show the incomplete coverage of the I-beam which was scanned from only one location, and gaps due to shadowing. Careful consideration must therefore be given to scanner survey planning for such projects [*Gordon et al.* 2001a].

The merged laser scanner point clouds gave a sampled representation of the bridge, from which member positions, lengths and cross-sections were extracted. Bridge members can also be interactively modelled using facilities offered by many software packages e.g. geometric form fitting of planes and cylinders. Form fitting can serve to complete members containing data gaps due to occlusions. However, these idealized shapes are not necessarily appropriate for irregularly shaped members such as a timber column, whose cross-section changes significantly along its length.

Curtin University Calibration Field

Another aspect of the authors' assessment of laser scanning for deformation monitoring has been simulated testing using a calibration target array. The Curtin University outdoor camera calibration field is an array of more than 100 retro-reflective targets affixed to the electrical engineering building on campus. With dimensions of 12 m by 10 m, the area of the field is ideally suited for ground-based laser scanner testing, save for the fact that most of the targets are confined to a vertical plane.

Simulated deformation testing was performed on the Cyrax 2400 in May 2000. The aim of the study was to quantify the sensitivity of the scanner for deformation detection. As shown in Figure 9, the scanner was mounted atop a precision vertical translation stage. The retro-reflective targets of the calibration field are visible in the background of the image. The building upon which they are mounted is constructed from red brick with mortar joints. One of the Cyra targets, consisting of a white circle centred on a green film backing, is visible atop the survey tripod in the centre of the image. Situated about 28 m from the field, the scanner was raised in known increments to simulate vertical subsidence of the building. A rendered view of a scan of the entire wall, illustrated in Figure 10, further illustrates the intricate level of detail that can be captured with a laser scanner. The moiré effect that appears on the building is due to the low display resolution of the image relative to the spatial frequency of the brickwork pattern.

Due to the high scan resolution (the sampling interval was approximately 15 mm in the plane of the wall), scan time was high so a subset of 25 targets was scanned. Data acquisition commenced

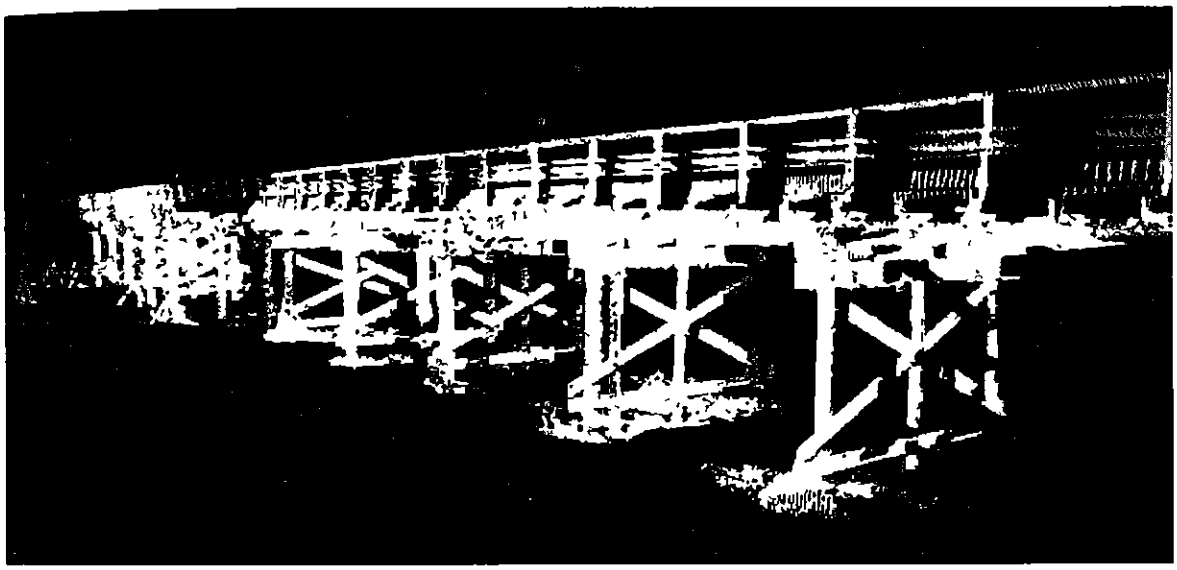

Figure 7: Toodyay bridge scan cloud mosaic.

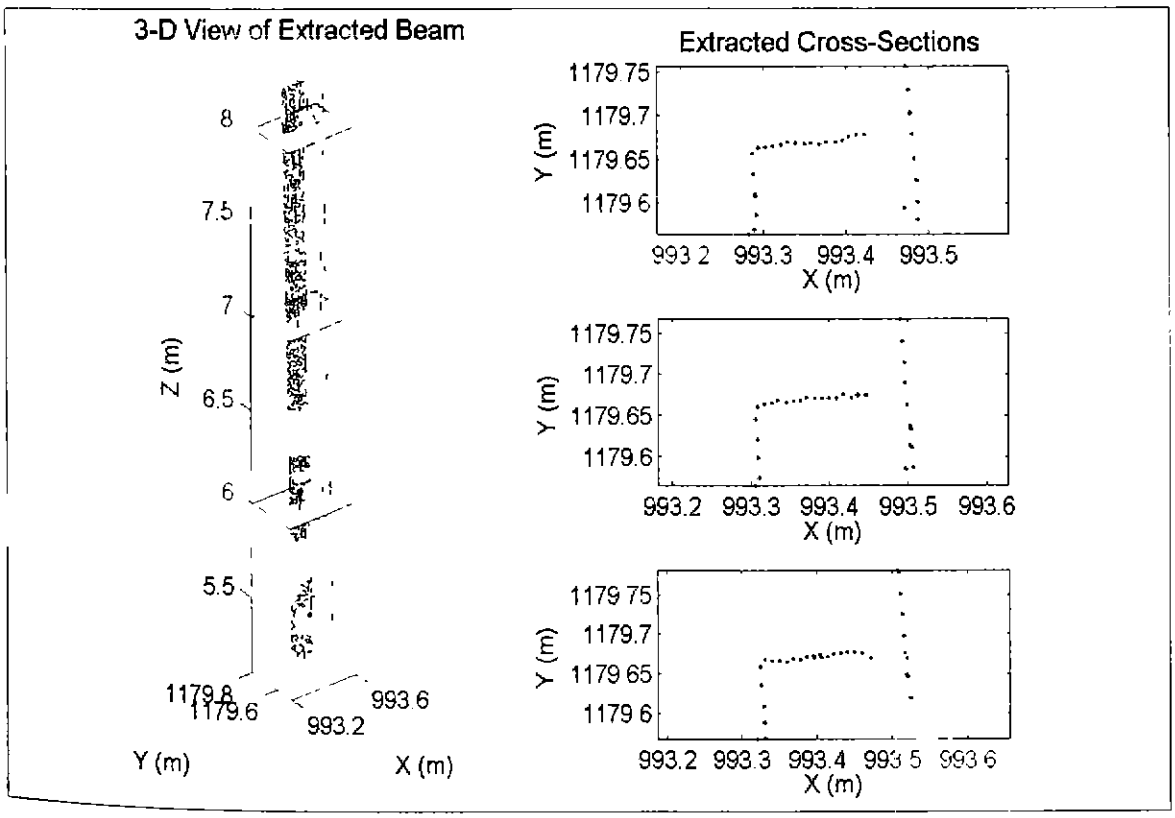

Figure 8: Extracted I-beam point cloud and cross-sections.

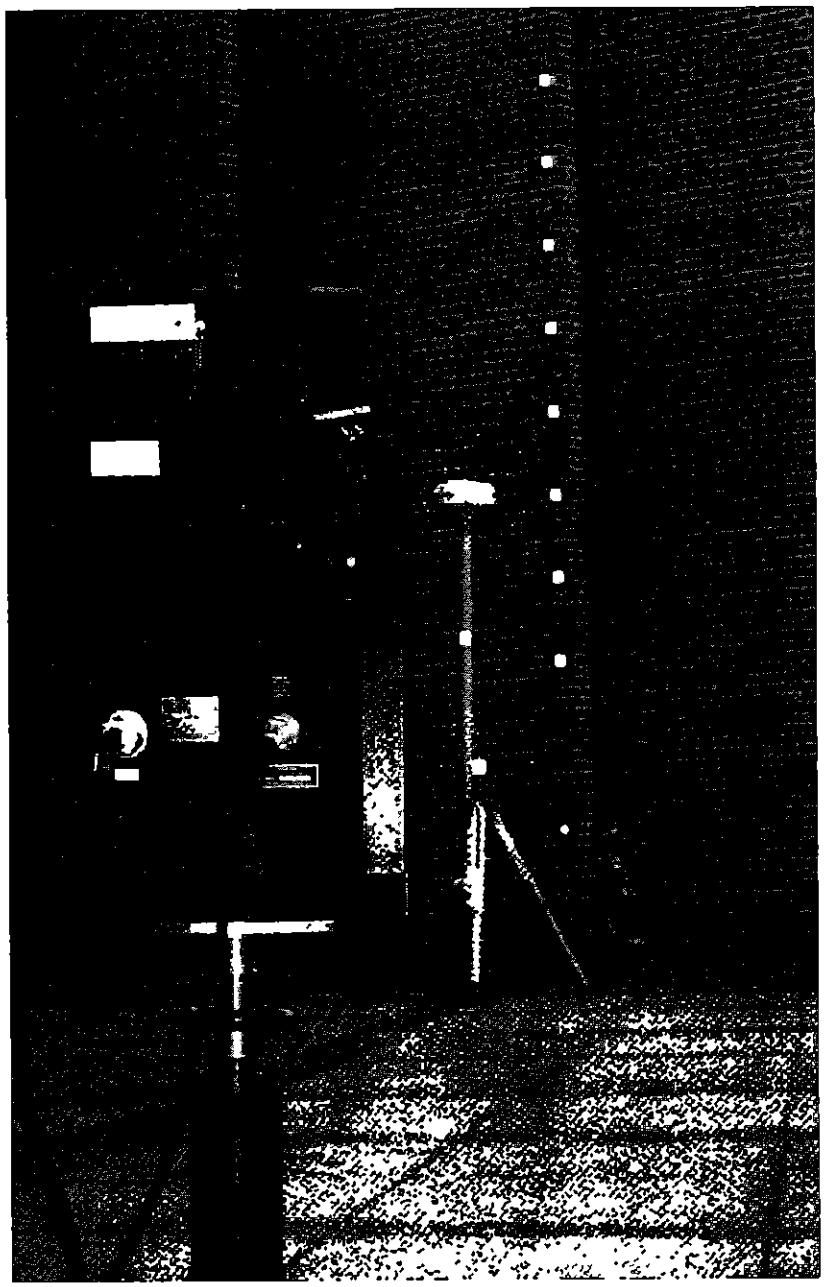

Figure 9: Cyrax 2400 scanner and calibration field

with a series of static scans for accuracy assessment followed by three epochs in which the scanner was raised by 5 mm (one complete turn of the translation stage) each time. The standard deviation of coordinate differences from the static epochs was ± 3 mm (1 σ) in the plane of the wall and ± 2 mm (1 σ) in the range (out of plane) dimension. These statistics were compiled from 135 point measurements.

The deformation vector plot from the third epoch (8.5 mm induced movement), shown in Figure 11, clearly indicates that a vertical motion was sensed by the scanner. Although this was indeed a large movement, the result was rather encouraging given the manufacturer's reported single-point accuracy of ± 6 mm. However, the vectors also reveal the presence of a horizontal systematic error, as they drift to the left of the figure. This is believed to be due to a combination of imperfect scanner levelling and centroid reduction error. Additional details about this experiment are found in *Gordon et al.* [2001b].

Figure 12 is an extracted portion of the scan cloud of the calibration field wall. While laser returns from the mortar joints are clearly visible, there are no responses from the red bricks, save for the occasional return due to possible material inhomogeneity. The same effect—lack of reflectance—was encountered with other materials, including a concrete walkway and a retaining wall constructed of reef limestone blocks. To determine the cause of this problem, the spectral reflectance signatures of these and other materials were measured using an IRIS Mk5 dual beam spectrometer.

Figure 10: Calibration wall scan cloud.

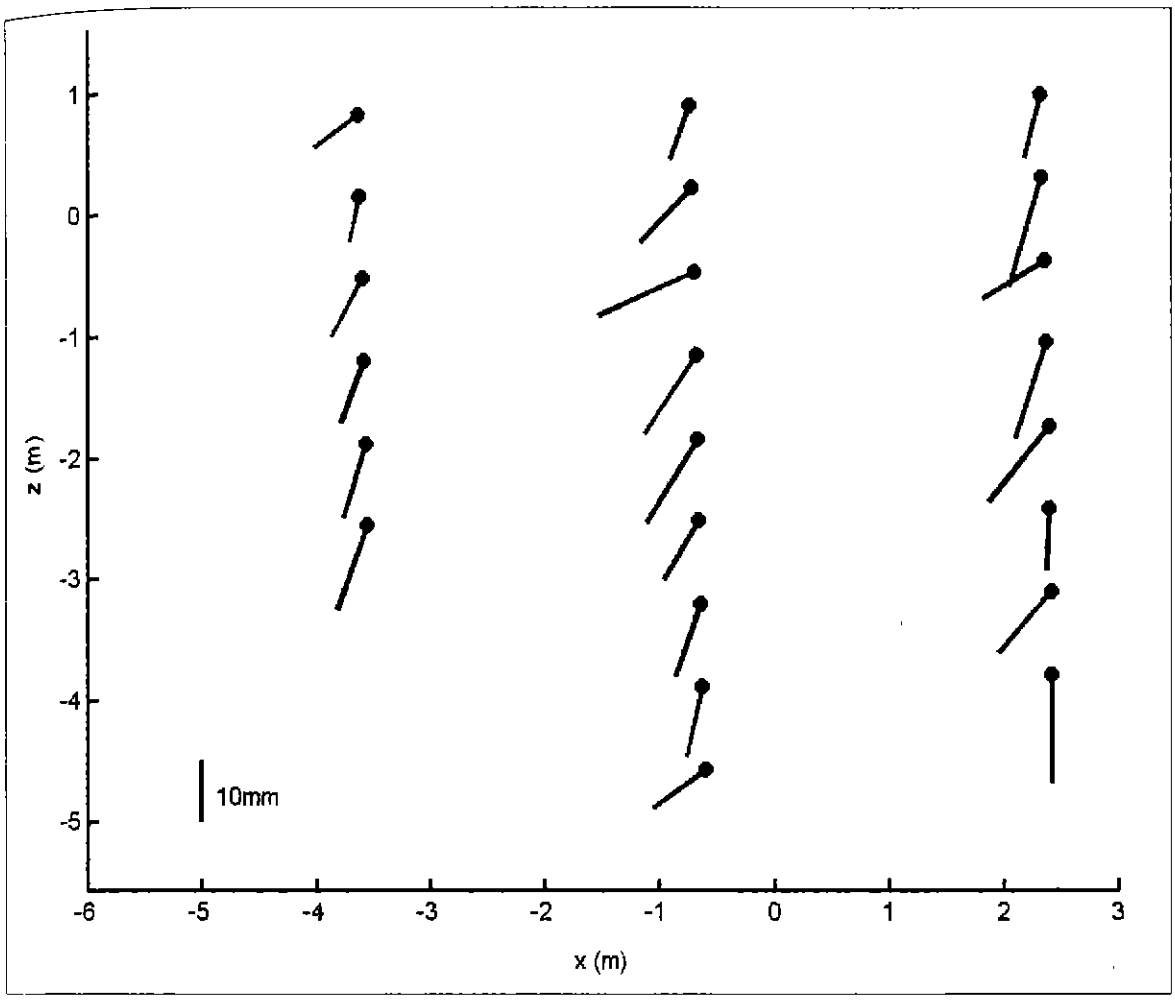

Figure 11: Recovered deformation vectors

Figure 13 shows the spectral reflectance signatures in the visible region of the electromagnetic spectrum for several different materials. The central wavelength of the Cyrax scanner (532 nm) is plotted as the dashed vertical line. Not surprisingly, the mortar exhibited strong (51%) reflectance at 532 nm, while the red brick reflected little green light (9%). The concrete and limestone specimens also exhibited low (20% and 15%, respectively) reflectance. The low magnitude of these curves at 532 nm helped to explain the lack of response from various materials.

Interesting, however, were the signatures for the Cyra target components. While the white centre material reflected highly (74%), as expected, the green target film exhibited only 16% reflectance at 532 nm. In two days of testing, strong returns were always received from the green film. Curiously, the peak reflectance of the green film was located toward the blue end of the spectrum, some 37 nm to the left of the laser central wavelength. Without knowledge of the system parameters such as laser line width, detector threshold, etc., it is impossible to speculate why the green film, which exhibited low reflectance at 532 nm, consistently produced strong returns.

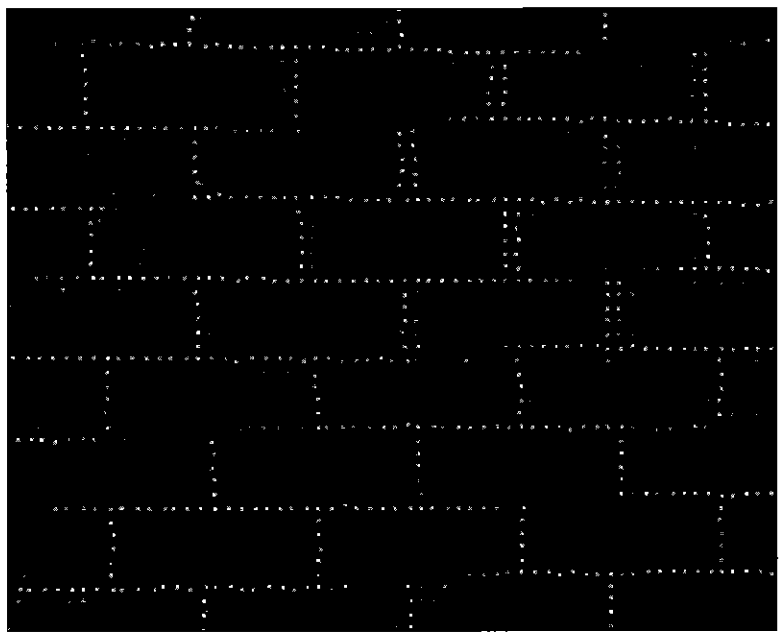

Figure 12: Brick and mortar wall laser returns.

Conclusions

Ground-based laser scanning offers great potential to the geomatics industry as a versatile tool for high-resolution spatial data capture, permitting

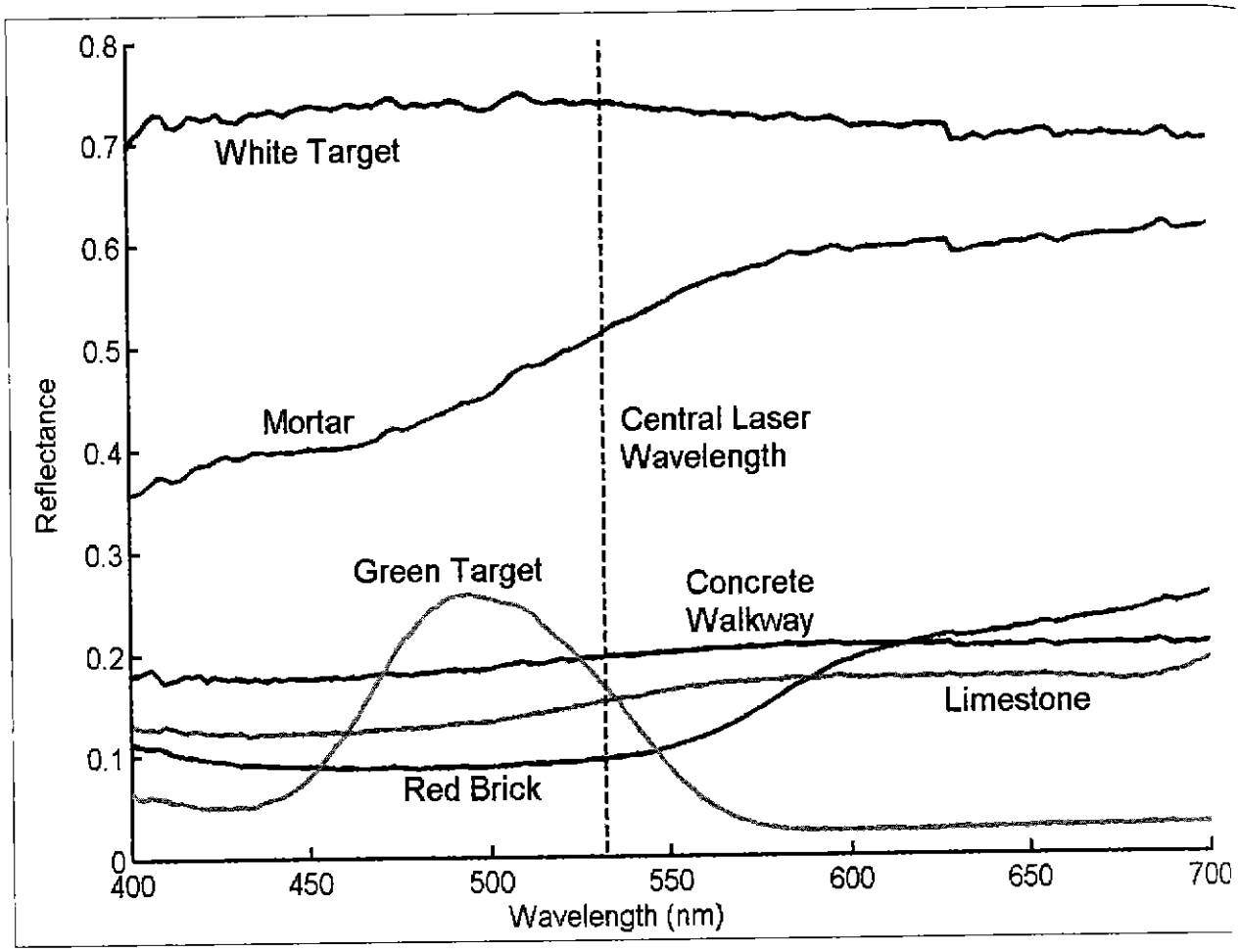

Figure 13: Measured spectral reflectance signatures.

rapid acquisition of unprecedented data volumes. As an emerging technology, ground-based laser scanning research is still in its infancy, which is evident in the lack of published work to date. An overview of ground-based laser scanner operation, commercially available systems and observables and transformations has been presented. A few projects conducted at Curtin University have been described to illustrate the practical use of laser scanning for monitoring applications.

Future avenues of research include further benchmark testing and calibration, further investigation into the effects of reflecting material properties, automated feature extraction and applications in structural assessment and monitoring. Accuracy and instrument calibration are issues of paramount importance to photogrammetrists, geodesists and surveyors. As mentioned previously, existing calibration practices are not directly applicable to laser scanners due to the fundamental difference in the method of measurement (uniform sampling instead of pointable measurement). Appropriate and tractable calibration procedures must therefore be developed to ensure the quality of scanner measurements. The effects of reflecting surface material on range measurements must also be quantified for quality assurance.

Laser scanners generate huge volumes of d of very intricate scenes like bridges. Extraction useful information, such as individual structu members and their dimensions, from these s clouds is both tedious and time consumi However, there is a need for automated feat extraction research that will strive to minimize user intervention required for this process.

Acknowledgements

The authors gratefully acknowledge the supp of the following organizations and individ throughout the course of this research: Maptek Ltd., Whelans Surveying and Mapping Pty. L Leica Geosystems Pty. Ltd. (Western Austra Diamond River Corporation, Cyra Technologies L Glenn Newnham, Tony Snow and Jonathon Dur

References

Baltsavias, E. P. 1999. Airborne laser scanning: b relations and formulas, *ISPRS Journal Photogrammetry and Remote Sensing*, 54: 199-

Beraldin, J. -A., F. Blais, P. Boulanger, L. Cournoyer, J. Domey, S. F. El-Hakim, G. Godin, M. Rioux and J. Taylor. 2000. Real world monitoring through high resolution digital 3D imaging of objects and structures, *ISPRS Journal of Photogrammetry and Remote Sensing*, 55: 230-250.

Callidus Precision Systems GmbH. 2001. URL: *http://www.callidus.de/rahm_en.htm.*

Cyra Technologies, Inc. 2001. URL: *http://www.cyra.com/.*

Fowles, G. R. 1975. *Introduction to Modern Optics*, Second Edition, New York, NY, Dover Publications Inc., 328 p.

Gordon, S. J., D. D. Lichti, M. P. Stewart and M. Tsakiri. 2001a. Metric performance of a high-resolution laser scanner, In *Videometrics and Optical Methods for 3D Shape Measurement*, 22-23 January 2001. 174-184.

Gordon, S. J., D. D. Lichti and M. P. Stewart. 2001b. Application of a high-resolution, ground-based laser scanner for deformation measurements, In *Proceedings of the 10th International Symposium on Deformation Measurements*, 19-22 March 2001, 23-32.

I-SiTE Ltd. 2001. URL: *http://www.isite3d.com/index.html.*

Jelalian, A. 1992. *Laser Radar Systems*, Boston, MA, Artech House, 292 p.

Lichti, D. D., M. P. Stewart, M. Tsakiri and A. J. Snow. 2000. Benchmark tests on a three-dimensional laser scanning system. *Geomatics Research Australasia*. 72: 1-23.

Marshall, G. F. (Ed.). 1985. *Laser Beam Scanning: Opto-Mechanical Devices, Systems and Data Storage Optics*, New York, NY, Marcel Dekker Inc, 423 p.

Matthews, L. and G. Garcia. 1995. *Laser and Eye Safety in the Laboratory*, Piscataway, NJ, IEEE Press, 156 p.

Optech Incorporated. 2001. URL: *http://www.optech.on.ca.*

RIEGL Laser Measurement Systems. 2001. URL: *http://www.riegl.co.at/.*

Wehr, A. and U. Lohr. 1999. Airborne laser scanning—an introduction and overview, *ISPRS Journal of Photogrammetry and Remote Sensing*, 54: 68-82.

Weichel, H. 1990. *Laser Beam Propagation in the Atmosphere*, Bellingham, WA, SPIE Optical Engineering Press, 98 p.

MS rec'd 01/06/12
Revised MS rec'd 02/01/15

Authors

Derek Lichti

Dr. Derek Lichti is Senior Lecturer in Photogrammetry at Curtin University of Technology. He holds a bachelor's degree in Survey Engineering from Ryerson University and MSc and PhD degrees in Geomatics Engineering from the University of Calgary. His research interests lie in the calibration and use of ground-based laser scanners and digital cameras for precision metrology applications.

Stuart Gordon

Stuart Gordon is a research student at the Department of Spatial Sciences, Curtin University of Technology. His research consists of assessing the performance of commercially available laser scanning systems and applying them to surveying tasks. In particular, he is investigating the potential of scanners for deformation monitoring.

Mike Stewart

Dr. Mike Stewart holds the position of Associate Professor in GPS/Geodesy at Curtin University. Educated at the Universities of Liverpool and Edinburgh in the United Kingdom, he held a four-year postdoctoral position at the University of Nottingham prior to taking an academic post in Australia in 1994. Surface deformation monitoring and GPS error analysis are among his current research interests. ❑